ACS Catalysis

Research Article

pubs.acs.org/acscatalysis

Ligand Effects on Reactivity of Cobalt Acyl Complexes

James M. Birbeck,[†] Anthony Haynes,*[,†] Harry Adams,[†] Llewellyn Damoense,[‡] and Stefanus Otto[‡]

[†]Department of Chemistry, University of Sheffield, Sheffield, S3 7HF, U.K.

[‡]Sasol Technology Research & Development, 1 Klasie Havenga Road, Sasolburg, 1947, South Africa

Supporting Information

ABSTRACT: Hydrogenolysis reactions of cobalt acyl complexes, $[Co(CO)_3(L)(COR)]$ (L = phosphine, R = Me, ^{n}Pr) have been monitored using in situ IR spectroscopy at moderate temperatures (<75 °C) and pressures (<25 bar). The reactions provide a model for the product-formation step in phosphine-modified, cobalt-catalyzed hydroformylation. The reaction kinetics are dependent on L, with the fastest rate being observed for the complex containing *n*-pentyl-9-phosphabicyclo[4.2.1]nonane (a_5-PhobPC$_5$). The observed dependence of rate on H_2 and CO pressure is consistent with a mechanism involving initial CO dissociation, followed by reaction of $[Co(CO)_2(L)(COR)]$ with H_2. Isotopic exchange experiments, monitored by IR spectroscopy, demonstrate that both terminal and acetyl carbonyls of $[Co(CO)_3(L)(COR)]$ exchange with free ^{13}CO. Kinetic data are also reported for reactions of $[Co(CO)_3(L)(COR)]$ with triphenyltinhydride. A zero-order dependence on $[Ph_3SnH]$ (at large excess) and positive values of $\Delta S^{\ddagger}$ demonstrate rate-determining CO dissociation. For a series of less bulky, symmetrical phosphines, the rates follow the sequence $PEt_3 < PMe_2Ph \sim PEtPh_2 < PPh_3 < P(4\text{-}ClC_6H_4)_3$, in accord with their electron-donating strength. Higher rates are found for more bulky phosphines, and the fastest rate is again found for L = a_5-PhobPC$_5$. Calculations using density functional theory indicate that the CO dissociation energy for $[Co(CO)_3(L)(COMe)]$ is influenced by the stereoelectronic properties of L, with steric bulk having a substantial effect. X-ray crystal structures are reported for $[Co(CO)_3(PEtPh_2)(COMe)]$, $[Co(CO)_3(s\text{-PhobPC}_5)]_2$, and $[Co(CO)_3(a_5\text{-PhobPC}_5)]_2$.

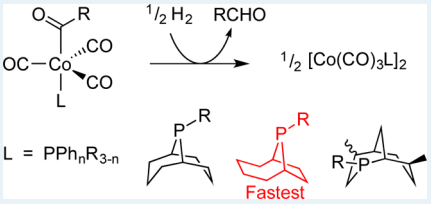

KEYWORDS: *hydroformylation, cobalt, phosphine, carbonyl, acyl, in situ IR, kinetics, mechanism*

INTRODUCTION

Hydroformylation of alkenes is one of the most important applications of homogeneous transition metal catalysis.[1−4] Large-scale processes based on both cobalt and rhodium catalysts have been commercialized to produce a range of aldehydes and alcohols, with applications including chemical intermediates, solvents, plasticizers, detergents, and surfactants.

Cobalt-catalyzed hydroformylation in the absence of phosphine ligands (termed "unmodified") typically operates at temperatures between 100 and 180 °C and syn-gas pressures of 100−300 bar. Addition of a phosphine ligand (such as P^{n}Bu$_3$ or P(octyl)$_3$) to give a "modified" system results in stabilization of the cobalt catalyst at lower CO partial pressure but lower intrinsic activity such that lower syn-gas pressures (<100 bar) but higher temperatures (160−220 °C) are employed.[5] Coordination of a phosphine increases the electron density on cobalt, which results in stronger binding of CO as well as enhanced hydrogenation activity. Hence, phosphine-modified cobalt catalysts are useful for production of alcohols, but with some loss of alkene feedstock by hydrogenation to the corresponding alkane. A significant benefit of phosphine-modified cobalt hydroformylation is the enhanced selectivity for more valuable linear aldehydes and alcohols, with linearities of up to 90% being achievable (compared wtih 45−55% for an unmodified catalyst).

The catalytic mechanism was originally established by Heck and Breslow[6] for the unmodified catalyst, but the same key steps also operate for modified systems. Hence, as shown in Scheme 1, a cobalt hydride species $[Co(CO)_3(L)H]$, generated in situ, loses a CO ligand to allow coordination and insertion of the alkene substrate. This gives a cobalt alkyl that undergoes migratory CO insertion to form an acyl. Hydrogenolysis of the acyl releases the aldehyde product and regenerates the active cobalt hydride. In the presence of added phosphine, both modified (L = PR$_3$) and unmodified (L = CO) cycles can occur, with relative contributions depending on reaction conditions and the properties of the phosphine ligand used.

Particularly good catalytic properties are exhibited by a class of bicyclic phosphine ligands known as phobanes (9-phosphabicyclononanes) introduced by Shell.[7] Three structural isomers can exist for a generic phobane (*s*-PhobPR, a_5-PhobPR and a_7-PhobPR, Chart 1), arising from radical addition of phosphine to 1,5-cycloocadiene. Mixtures of the symmetrical and unsymmetrical isomers are generally used industrially, since separation would increase cost. However, methods for their separation have been developed, and the three isomers have been shown to have significantly different properties, with donor strength decreasing in the sequence $a_7 > s > a_5$ and steric bulk following the reverse order.[8−11] Recent studies[12,13] have assessed the influence of phobane ligands on cobalt-catalyzed

Received: September 6, 2012
Revised: October 17, 2012
Published: October 22, 2012

   dx.doi.org/10.1021/cs300589n | ACS Catal. 2012, 2, 2512−2523

Scheme 1. Cycle for Cobalt Catalyzed Alkene Hydroformylation[a]

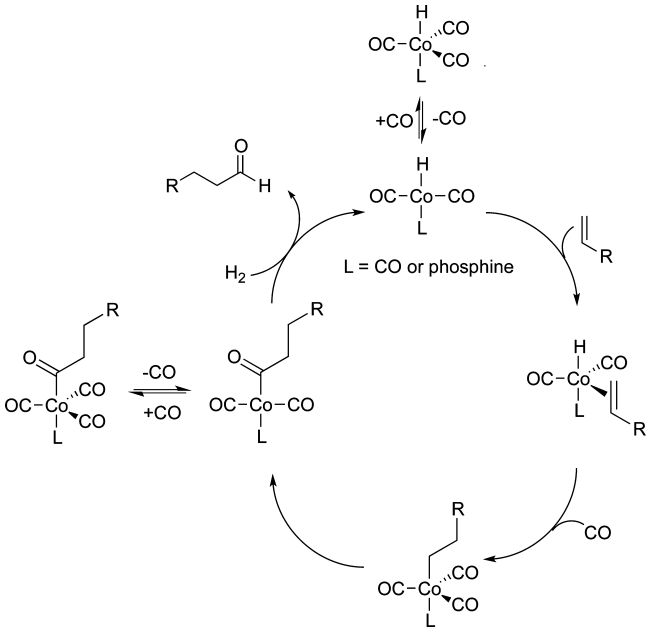

[a]The parallel pathway to branched aldehyde product is omitted.

Chart 1. Structures of Phobane and Limonene-Derived Phosphine Ligands

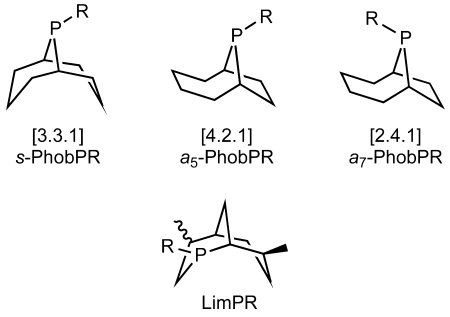

hydroformylation and showed the *s*-PhobPEt ligand to be more strongly coordinating than the a_5-PhobPEt isomer, with the latter requiring slightly higher ligand concentration to achieve fully modified catalysis. Other bicyclic phosphine ligands, derived from limonene (LimPR, Chart 1), have also received attention in recent years.[14−19]

In situ spectroscopy has been used widely to develop mechanistic understanding of cobalt-catalyzed hydroformylation. The literature on this subject was reviewed in 2004 by Damoense et al.[18] Both high-pressure IR (HPIR) and NMR spectroscopic methods have been used to probe cobalt carbonyl species, yielding information concerning equilibria between modified and unmodified catalyst species and formation of hydrides $[Co(CO)_3(L)H]$ from dimers $[Co(CO)_3(L)]_2$ under catalytic conditions.[16,20−25]

In this paper, we report a kinetic investigation of the stoichiometric hydrogenolysis of some cobalt acyls, $[Co(CO)_3(L)(COR)]$, using HPIR spectroscopy at temperatures and pressures below those typically used for catalytic hydroformylation. The hydrogenolysis data are supplemented by studies of carbonyl ligand exchange with ^{13}CO and kinetic measurements for model reactions of cobalt acyls with triphenyltinhydride. It was of particular interest to quantify the effects of a variety of phosphine ligands on reactivity, especially for the PhobPR and LimPR ligands that have shown beneficial behavior in catalysis. Notably, we find that the highest reactivity occurs for the cobalt complex containing the a_5-$PhobPC_5$ ligand. The results are interpreted on the basis of ligand electronic and steric effects on the rate of CO dissociation from the cobalt center. The experimental results are supported by DFT calculations on Co−CO dissociation energies.

RESULTS AND DISCUSSION

Synthesis and Characterization of Cobalt Acyl Complexes. Cobalt acyl complexes $[Co(CO)_3(L)(COR)]$ were synthesized by established methods, involving reaction of $Na[Co(CO)_4]$ with an alkyl iodide to give the alkyl complex $[Co(CO)_4R]$ and subsequent addition of the phosphine L. In the case of R = ^{n}Pr, it was found that this method resulted in some of the isomeric product containing a CO^{i}Pr moiety; therefore, alternative routes involving acylation of $Na[Co(CO)_4]$ or $Na[Co(CO)_3L]$ with *n*-butyryl chloride were employed.

The product complexes were characterized by IR, ^1H NMR, and ^{31}P NMR spectroscopy. All show the expected pattern of $\nu(CO)$ absorptions in the IR spectrum with a low frequency band at ∼1660 cm^{-1} due to the acetyl ligand. The terminal $\nu(CO)$ region shows a weak high frequency band due to the symmetric A_1 $\nu(CO)$ mode (∼2040 cm^{-1}) and a stronger pair of absorptions (split by 18−20 cm^{-1}) due to the split "E" mode of the $Co(CO)_3$ fragment, for which strict C_3 symmetry is lost due to the presence of the acyl ligand. The observed $\nu(CO)$ values depend on the donor strength of the phosphine ligand, L, according to expectation. Hence, for the terminal $\nu(CO)$ bands, the observed frequencies decrease in the order L = $P(p\text{-}ClC_6H_4)_3$ > PPh_3 > $PMePh_2$ > $PEtPh_2$ ∼ PMe_2Ph > PEt_3 > P^nBu_3 > PCy_3. The PhobPR and LimPR ligands (R = *n*-pentyl, or dodecyl, denoted as C_5/C_{18}) give $\nu(CO)$ frequencies comparable to those for L = PEt_3 and P^nBu_3. Notably, *s*-$PhobPC_5$ is a marginally better donor than a_5-$PhobPC_5$, giving a shift in $\nu(CO)$ to low frequency of ∼2 cm^{-1}, which is consistent with previous studies.[10,11] For the complexes containing the $LimPC_5$ or $LimPC_{18}$ ligands, two ^{31}P NMR resonances were observed, arising from the presence of two diastereoisomers of the phosphine ligand, as discussed previously by Crause et al.[16]

Crystals of $[Co(CO)_3(PEtPh_2)(COMe)]$ suitable for an X-ray crystallographic study were obtained, and the molecular structure is shown in Figure 1. The complex adopts a distorted trigonal bipyramidal geometry with axial acetyl and phosphine ligands, in common with the structures of a number of complexes of this type that have been reported previously (e.g., for L = PPh_3, $P(o\text{-tolyl})_3$, PMe_2Ph, $P(4\text{-}FC_6H_4)_3$, PCy_3, $P(3\text{-}FC_6H_4)_3$).[26−28] The metal−ligand bond distances for $[Co(CO)_3(PEtPh_2)(COMe)]$ are very similar to those for other members of the series, but it is notable that the Co−P distances for the $P(o\text{-tolyl})_3$ and PCy_3 variants (∼2.31 and 2.28 Å, respectively) are somewhat longer than the average for the remainder (∼2.25 Å). This presumably reflects greater steric congestion.

Hydrogenolysis. The reaction of hydrogen (20 bar) with $[Co(CO)_3(P^nBu_3)(COMe)]$ to form acetaldehyde was reported in 1967 by Piacenti et al.[29] It was subsequently reported by Martin and Baird that $[Co(CO)_3(PMePh_2)(COMe)]$

dx.doi.org/10.1021/cs300589n | ACS Catal. 2012, 2, 2512−2523

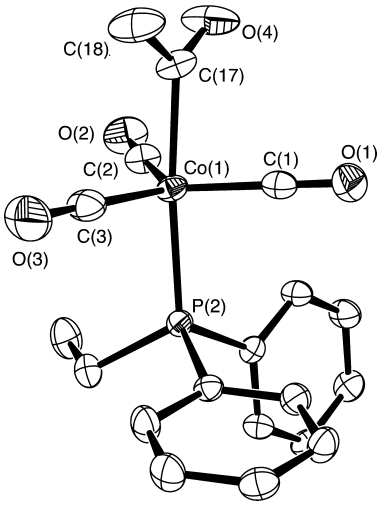

Figure 1. ORTEP diagram showing the molecular structure of $[Co(CO)_3(PEtPh_2)(COMe)]$. Thermal ellipsoids are shown at the 50% probability level, and hydrogen atoms are omitted. Selected bond distances (Å): Co1–C1, 1.788(3); Co1–C2, 1.795(2); Co1–C3, 1.791(2); Co1–C17, 2.010(2); Co1–P2, 2.2510(7); C17–C18, 1.511(3); C17–O4, 1.201(3). Selected bond angles (°): C17–Co1–P2, 174.56(9); C17–Co1–C1, 83.19(11); C17–Co1–C2, 84.85(10); C17–Co1–C3, 92.71(10); P2–Co1–C1, 91.37(7); P2–Co1–C2, 97.75(7); P2–Co1–C3, 90.45(8); C1–Co1–C2, 120.77(11); C2–Co1–C3, 115.90(13); C3–Co1–C1, 122.44(11).

undergoes hydrogenolysis within minutes at 35 bar H_2, although no reaction occurred at 1 bar H_2.[30] The only cobalt-containing product was the dimer, $[Co(CO)_3(PMePh_2)]_2$, resulting from elimination of molecular hydrogen from the presumed initial hydride, $[Co(CO)_3(PMePh_2)H]$, which is stable only at higher H_2 pressures (Scheme 2).

Scheme 2. Hydrogenolysis of $[Co(CO)_3(L)(COR)]$

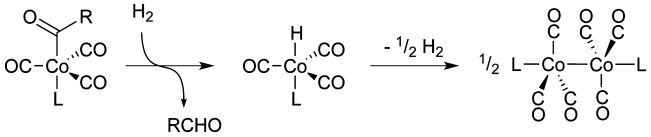

To our knowledge, quantitative kinetic data have not been reported for reactions of phosphine-modified cobalt acyls with H_2, but data are available for unmodified systems. Kovacs et al. studied the rate of hydrogenolysis of $[Co(CO)_4(COR)]$ (R = ^{n}Pr or ^{i}Pr) in *n*-heptane and found the results to be consistent with a mechanism involving initial CO loss, as depicted in the catalytic cycle in Scheme 1.[31] Rate constants for the CO dissociation step were found to be 0.023 and 0.047 s^{-1} respectively for the *n*-butyryl and iso-butyryl complexes at 25 °C.

In the present study, reactions of cobalt acyl complexes $[Co(CO)_3(L)(COR)]$ with hydrogen were monitored by in situ high-pressure IR spectroscopy using a cylindrical internal reflectance (CIR) cell of the type developed by Moser.[32−36] Reactions were carried out using toluene as solvent at temperatures up to ∼70 °C and H_2 pressures up to ∼20 bar. A typical set of IR spectra, for the reaction of $[Co(CO)_3(PEtPh_2)(COMe)]$ with H_2 at 52 °C is shown in Figure 2. The decay of the reactant ν(CO) bands is accompanied by

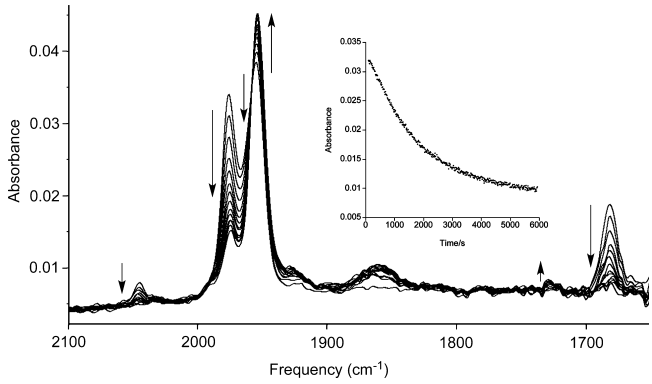

Figure 2. Series of IR spectra during the reaction of $[Co(CO)_3(PEtPh_2)(COMe)]$ with H_2 (6 bar) at 52 °C. Inset: plot of absorbance versus time for ν(CO) band at 1976 cm^{-1}.

the growth of a strong absorption at 1952 cm^{-1}, almost coincident with the low frequency terminal ν(CO) band of the reactant. This product band is assigned to the dimer, $[Co(CO)_3(PEtPh_2)]_2$, which was also identified by subsequent ^{31}P NMR spectroscopy (δ 63.2 in $CDCl_3$), which is consistent with the reaction sequence shown in Scheme 2, as reported previously by Martin and Baird.[30] Formation of acetaldehyde was evident from a very weak ν(CO) absorption at 1729 cm^{-1}, although some loss into the vapor phase probably occurs. Control experiments demonstrated that the cobalt acyl complexes were stable at elevated temperature under an inert (N_2) atmosphere over the time scale of these experiments, and the spectroscopic changes shown in Figure 2 occurred only once a pressure of H_2 was admitted to the CIR cell.

Similar observations were made for reactions of a range of cobalt acyl complexes. For complexes containing triaryl phosphines, such as PPh_3, issues with low solubility of the dimeric product were encountered. Hence, as the reaction proceeded, precipitation of the dimer onto the silicon rod of the CIR cell resulted in growth of an intense IR absorption at ∼1950 cm^{-1} associated with solid $[Co(CO)_3(PPh_3)]_2$. This precluded the determination of useful kinetic data for complexes containing triaryl phosphines (although a model reaction using Ph_3SnH proved useful in these cases; see below).

Kinetic analysis was performed by plotting of absorbance versus time for the higher frequency component of the intense split *E* ν(CO) mode of $[Co(CO)_3(L)(COMe)]$, which has minimal overlap with the product absorption. A typical plot (Figure 2, inset) is well fitted by an exponential decay curve ($A_t = A_\infty + (A_0 - A_\infty)e^{-k_{obs}t}$), leading to a pseudo-first-order rate constant, k_{obs}, for each kinetic experiment (tabulated in the Supporting Information). The observed rate constants are approximately proportional to H_2 pressure, as illustrated by plots of k_{obs} versus pH_2 for the complexes with L = $PEtPh_2$ and *s*-PhobPC$_5$ in Figure 3. Addition of CO caused a marked inhibition of hydrogenolysis rate. For example, k_{obs} values of 4.2 × 10^{-3} and 3.4 × 10^{-4} s^{-1} were found, respectively, when using 10.5 bar H_2 or 8.5:2.5 bar H_2/CO in reactions of $[Co(CO)_3(PMePh_2)(COMe)]$ (71 °C). The kinetic behavior is therefore consistent with the established mechanism for hydrogenolysis of $[Co(CO)_3(L)(COR)]$ species, involving reversible CO dissociation followed by activation of H_2 (Scheme 3), leading to the rate expression in eq 1.

dx.doi.org/10.1021/cs300589n | *ACS Catal.* 2012, 2, 2512−2523

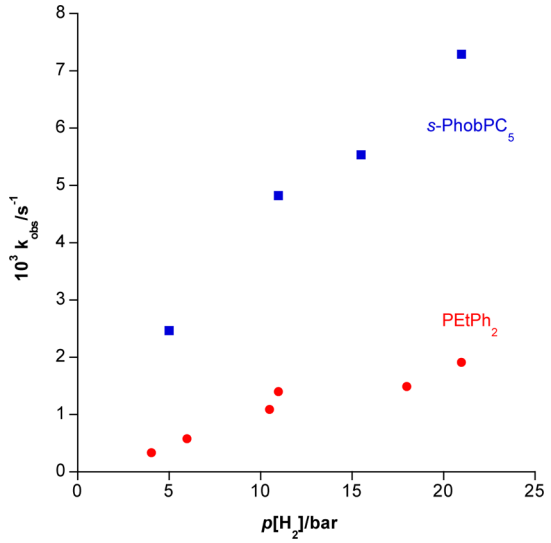

Figure 3. Plots of k_{obs} vs pH_2 for hydrogenolysis of $[Co(CO)_3(L)(COMe)]$ (L = $PEtPh_2$, *s*-$PhobPC_5$) in toluene, 52 °C.

$$\text{rate} = k_{obs}[Co(CO)_3(L)(COR)] \quad \text{where}$$
$$k_{obs} = k_1k_2[H_2]/(k_{-1}[CO] + k_2[H_2]) \qquad (1)$$

Scheme 3. Mechanism for Hydrogenolysis of $[Co(CO)_3(L)(COR)]$[a]

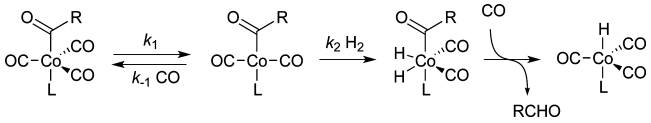

[a]For simplicity, the addition of H_2 to give a Co(III) dihydride is depicted as a single step, but theoretical calculations indicate the intermediacy of an η^2-H_2 complex prior to H_2 cleavage.[37−39]

If CO competes effectively with H_2 for the 16-electron intermediate, $[Co(CO)_2(L)(COR)]$, then a first-order dependence on $[H_2]$ will result ($k_{obs} \approx k_1k_2[H_2]/(k_{-1}[CO])$. However, if H_2 addition dominates over the reverse reaction, saturation kinetics will result, with a zero-order dependence on $[H_2]$ at high H_2 pressure (limiting $k_{obs} = k_1$). Under the conditions used in this study, it is apparent that the former situation applies.

Notably, the observed reactivity at a fixed H_2 pressure showed a marked dependence on the nature of the phosphine ligand L (Table 1). Whereas the k_{obs} values varied over a relatively small range for most of the complexes (L = PBu_3, $PEtPh_2$, $PMePh_2$, $LimPC_n$), significantly faster rates were found for L = PMe_2Ph and *s*-$PhobPC_5$ and especially for L = a_5-$PhobPC_5$. The large difference in k_{obs} (by a factor of 3) for the two phobane isomers is of particular interest, as discussed later. Changing the acyl group from COMe to CO^{n}Pr had only a relatively small effect on reactivity.

Variable temperature kinetic measurements were performed to determine apparent activation parameters for the hydrogenolysis reactions. Since the concentration of dissolved H_2 depends on temperature, this had to be accounted for in the construction of Eyring plots. Thus, the k_{obs} values obtained at a particular temperature were divided by the H_2 concentration in toluene at that temperature, calculated from literature data[40] (assuming a first-order dependence of k_{obs} on $[H_2]$). Activation parameters derived from Eyring plots of these data are given in Table 1. The activation enthalpies range from ∼50 to 95 kJ mol^{-1}, and the activation entropies vary in magnitude and sign. Mechanistic interpretation of these data is not straightforward because the apparent second-order rate constants being plotted do not correspond to a single reaction step but will have contributions from k_1, k_{-1}, and k_2 in Scheme 3. A more negative $\Delta S^{\ddagger}$ value presumably results from a more significant contribution from the associative H_2 addition step. The use of a model reaction to obtain kinetic data for the CO dissociation (k_1) step is described later in this paper.

Table 1. Observed Rate Constants k_{obs} (52 °C, 11 bar H_2) and Activation Parameters for Hydrogenolysis of $[Co(CO)_3(L)(COR)]$[a]

L	10^3 k_{obs}/s^{-1}	$\Delta H^{\ddagger}$/kJ mol^{-1}	$\Delta S^{\ddagger}$/J mol^{-1} K^{-1}
$PMePh_2$	1.3	50 ± 6	−100 ± 18
$PEtPh_2$	1.25	71 ± 5	−34 ± 16
PMe_2Ph	3.8	73 ± 11	−24 ± 34
P^nBu_3	0.95		
s-$PhobPC_5$	4.8	74 ± 8	−13 ± 24
a_5-$PhobPC_5$	14.6	83 ± 2	22 ± 4
$LimPC_5$	1.65	70 ± 4	−36 ± 10
$LimPC_{18}$	1.35	97 ± 2	44 ± 5
s-$PhobPC_5$ (R = ^{n}Pr)	5.6		
$LimPC_{18}$ (R = ^{n}Pr)	1.5		

[a]R = Me except where stated.

The most notable aspect of these results is the relatively high reactivity of the phobane complexes and also the significantly different hydrogenolysis rates for the *s*-$PhobPC_5$ and a_5-$PhobPC_5$ ligand isomers. On the basis of the mechanism in Scheme 3, the reactivity of a given complex will be controlled by a combination of the CO dissociation rate constant, k_1, and the ratio $k_2[H_2]/k_{-1}[CO]$, which determines the fate of the 16-electron intermediate. Clearly, the properties of the phosphine spectator ligand will influence each of these rate constants. The rate of CO loss is expected to be related to the Co−CO bond dissociation energy, which will depend on the strength of π-backbonding from the metal center. Hence, more strongly donating phosphine ligands will tend to discourage CO loss. However, steric effects will also contribute, and a bulky phosphine ligand can favor CO dissociation due to relief of steric congestion. Ligand stereoelectronic effects will also influence the reverse reaction with CO and the addition of H_2. Although the *s*-$PhobPC_5$ and a_5-$PhobPC_5$ isomers are known to have slightly different donor abilities,[10,11] they are both relatively strong donor ligands with ν(CO) values for $[Co(CO)_3(L)(COMe)]$ similar to those for L = P^nBu_3. Therefore the higher reactivity of the phobane complexes more likely results from steric factors, since they have much larger cone angles (e.g., 163° for *s*-$PhobPC_5$)[12] than P^nBu_3 (132°). On this basis, the relatively fast hydrogenolysis found for L = PMe_2Ph (cone angle 122°) appears to be anomalous, but it is possible that this results from more competitive H_2 addition (i.e., higher $k_2[H_2]/k_{-1}[CO]$) for this system.

^{13}CO Isotopic Exchange. Since a CO dissociation mechanism is implicated for the hydrogenolysis reactions discussed above, we performed some experiments using ^{13}CO to monitor the rate of exchange of bound and free CO in $[Co(CO)_3(L)(COMe)]$ (L = PPh_3 and *s*-$PhobPC_5$). For these experiments, a solution of the complex in 1,2-dichloroethane was stirred under 1 atm of ^{13}CO at 50 °C, and a small sample

dx.doi.org/10.1021/cs300589n | ACS Catal. 2012, 2, 2512−2523

was withdrawn periodically to measure the IR spectrum. A typical set of IR spectra for $[Co(CO)_3(PPh_3)(COMe)]$ is shown in Figure 4. The terminal ν(CO) bands of the unlabeled

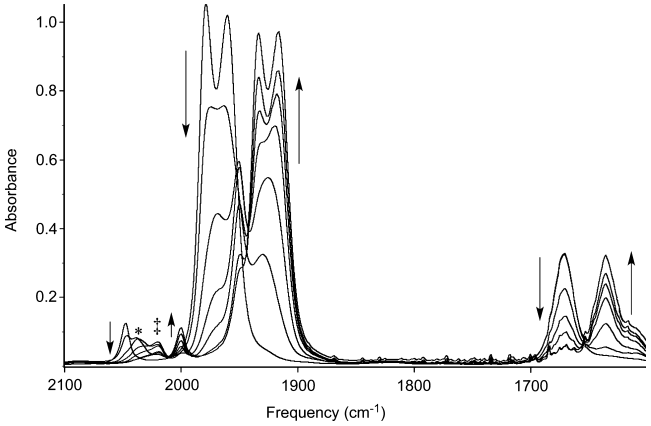

Figure 4. Series of IR spectra during the reaction of $[Co(CO)_3(PPh_3)(COMe)]$ with ^{13}CO (1 atm, 50 °C in 1,2-dichloroethane). Terminal ν(CO) bands due to intermediate ^{13}CO-substitituted species are indicated by * (mono-^{13}CO) and ‡ (bis-^{13}CO).

starting complex at 2048, 1978, and 1960 cm^{-1} decay over time to be replaced by a set of new bands at 2000, 1933, and 1916 cm^{-1} with the same intensity pattern but shifted to low frequency, which is consistent with substitution of the terminal CO ligands by ^{13}CO. The acyl ν(CO) band of $[Co(CO)_3(PPh_3)(COMe)]$ at 1671 cm^{-1} also decays, being replaced by an absorption at 1635 cm^{-1}, indicating that ^{13}CO is also incorporated into the acetyl ligand. Qualitatively similar observations were made for an analogous experiment using $[Co(CO)_3(s\text{-}PhobPC_5)(COMe)]$.[41] During these experiments, additional absorptions were observed that can be assigned to species resulting from stepwise substitution of the three terminal CO ligands. Hence, for $[Co(CO)_3(PPh_3)(COMe)]$, the weak high-frequency ν(CO) bands of the mono- and bis-^{13}CO species were observed sequentially at 2038 and 2020 cm^{-1}. Identification of the more intense ν(CO) bands of these intermediates was hindered by overlapping absorptions in the region between 2000 and 1900 cm^{-1}.

The rate of CO ligand exchange was assessed by analyzing the decay of the high-frequency ν(CO) band of $[Co(CO)_3(L)(COMe)]$, which showed insignificant overlap with intermediate bands. Good exponential decay fits were obtained, giving first-order rate constants of 7×10^{-4} and 1.2×10^{-3} s^{-1} for L = PPh_3 and *s*-$PhobPC_5$, respectively (corresponding to half-lives of 1050 and 625 s). Hence, these data are consistent with a faster CO dissociation from the *s*-$PhobC_5$ complex than from the PPh_3 complex. It is noteworthy that the CO-exchange rates for these phosphine-substituted cobalt acyl complexes are much slower (~50 times) than those previously reported for $[Co(CO)_4R]$ (R = CH_2CO_2Me, CO_2Et) (based on values extrapolated to 50 °C using reported activation parameters).[42] This exemplifies the inhibiting effect of phosphine ligands on CO lability.

These experiments also show that ^{13}CO becomes incorporated into the acetyl ligand of $[Co(CO)_3(L)(COMe)]$, indicating that reversible alkyl migration to the cobalt center can occur (as shown in Scheme 4) to generate a $^{13}COMe$ moiety. Absorbance vs time plots (in the Supporting Information) reveal an induction period for formation of the

Scheme 4. Mechanism for CO Exchange of Terminal and Acyl Carbonyls in $[Co(CO)_3(L)(COR)]$

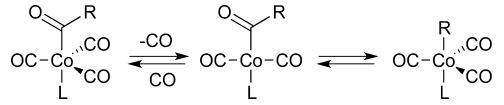

$^{13}COMe$ species. This arises because ^{13}CO must accumulate in the terminal carbonyl sites before a labeled acetyl moiety can be formed by the mechanism in Scheme 4. The competition between alkyl migration and CO coordination in coordinatively unsaturated $[Co(CO)_2(L)(COMe)]$ (L = PPh_3, P^nBu_3) has been quantified previously in a study by Ford and co-workers using flash photolysis coupled with fast time-resolved IR spectroscopy.[43]

Model Reactions with Ph_3SnH. To probe CO dissociation from $[Co(CO)_3(L)(COR)]$ in isolation (and so to determine the effect of L on this step), a reaction was sought in which the unsaturated intermediate resulting from CO loss is trapped more efficiently than by H_2. Related cobalt–acyl cleavage reactions have been reported previously using group 14 hydrides R_3EH (E = Si, Sn). Wegman investigated the reactions of both silanes and stannanes with $[Co(CO)_3(PPh_3)(COMe)]$ and found more simple kinetic behavior for the stannane reactions, which were first-order in reactant complex and zero-order in stannane.[44] This was interpreted on the basis of a mechanism involving CO dissociation (Scheme 5) analogous to that for hydrogenolysis but with more effective scavenging of the $[Co(CO)_2(PPh_3)(COMe)]$ intermediate by the stannane. For silanes, the observed rates depended on R_3SiH concentration, indicating that addition of the Si–H bond to cobalt is not so rapid as the corresponding Sn–H addition (although it is faster than H_2 addition). Gregg and Cutler also investigated the reactions of silanes with cobalt acyl complexes and reported additional mechanistic complexity.[45] On the basis of these reports and our preliminary experiments with both silanes and stannanes, we selected the reactions of $[Co(CO)_3(L)(COR)]$ with Ph_3SnH as suitable to determine the effect of L on CO dissociation rate.

The reactions of cobalt acyl complexes with Ph_3SnH were monitored by in situ IR spectroscopy under pseudo-first-order conditions (excess stannane). Since high pressures were not necessary for these reactions, a simple thermostatted IR transmission cell was utilized. A wider range of complexes was amenable to study in this part of the investigation, since product precipitation was not problematic under the conditions used for these experiments. The transmission IR cell used has a much longer path length (0.5 mm) than the effective path length of the high-pressure CIR cell used for the hydrogenolysis reactions, so a considerably lower concentration of cobalt complex can be used. This meant that complexes of triarylphosphines, which formed sparingly soluble dimeric products in the hydrogenolysis study, could be included in the data set for the stannane reactions.

A typical set of spectra, for the reaction of $[Co(CO)_3(LimPC_{18})(COMe)]$ with Ph_3SnH in THF (46 °C) is shown in Figure 5. The bands of the reactant complex at 2040, 1969, 1947, and 1676 cm^{-1} all decay, and a strong band appears at 1942 cm^{-1} due to the product cobalt stannyl complex, $[Co(CO)_3(LimPC_{18})(SnPh_3)]$. Formation of acetaldehyde is also apparent from the band that grows at 1727 cm^{-1}. A plot of absorbance versus time for the strong reactant ν(CO) band at 1969 cm^{-1} is well fitted by an exponential decay curve to give a

dx.doi.org/10.1021/cs300589n | ACS Catal. 2012, 2, 2512–2523

Scheme 5. Mechanism for Reaction of $[Co(CO)_3(L)(COR)]$ with Ph_3SnH

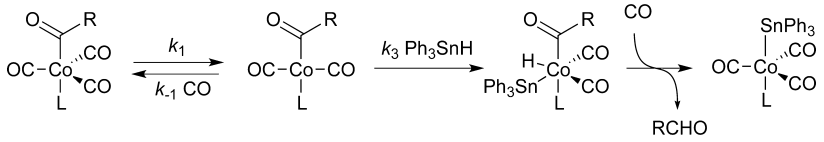

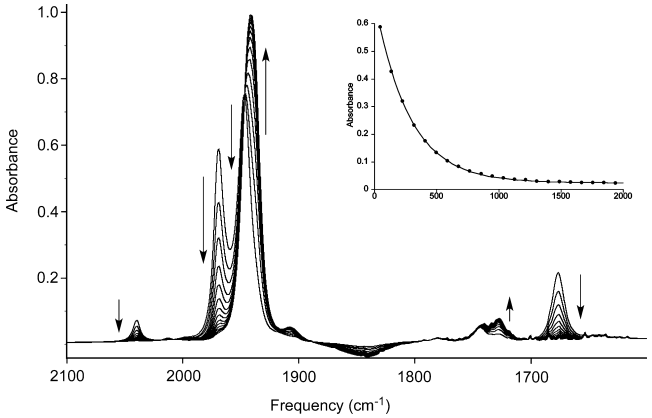

Figure 5. Series of IR spectra during the reaction of $[Co(CO)_3(LimPC_{18})(COMe)]$ with Ph_3SnH in THF (46 °C). The broad negative absorption near 1850 cm^{-1} is due to depletion of Ph_3SnH. Inset: plot of absorbance versus time for ν(CO) band at 1969 cm^{-1}.

pseudo-first-order rate constant, k_{obs}. Values of k_{obs} for reactions of a series of cobalt acyl complexes under a range of conditions are listed in the Supporting Information. As reported by Wegman,[44] k_{obs} for the reaction of $[Co(CO)_3(PPh_3)(COMe)]$ is independent of Ph_3SnH concentration over the range 0.07−0.59 mol dm^{-3}. Hence, on the basis of the mechanism shown in Scheme 5, the k_{obs} values can be equated with the rate constant for CO dissociation, k_1.

Data showing the effect of the phosphine L on reaction rate are shown in Table 2. It is clear that the most reactive member of the series is the a_5-$PhobPC_5$ complex, as in the hydrogenolysis reactions; however, the precise order is somewhat different, with the $LimPC_{5/18}$ complexes now marginally faster than the *s*-$PhobPC_5$ complex, and the PMe_2Ph complex lower down the reactivity series. This supports the suggestion made earlier that the relatively high hydrogenolysis rate for $[Co(CO)_3(PMe_2Ph)(COMe)]$ results from faster H_2 addition to the CO-loss intermediate (relative to the back reaction with CO). The ratio of rates for reactions of the PPh_3 and *s*-$PhobPC_5$ complexes with Ph_3SnH (1:1.6) is similar to the corresponding ratio for the ^{13}CO exchange reactions reported above (1:1.7), although the solvent and temperature differ for the two sets of data.

Table 2. Observed Rate Constants k_{obs} (74 mM, THF, 40 °C) and Activation Parameters for Reactions of $[Co(CO)_3(L)(COR)]$ with Ph_3SnH[a]

L	$10^3\ k_{obs}/s^{-1}$	$\Delta H^{\ddagger}$/kJ mol^{-1}	$\Delta S^{\ddagger}$/J mol^{-1} K^{-1}
PPh_3	0.89	110 ± 1	50 ± 2
$P(4\text{-}ClC_6H_4)_3$	1.37	111 ± 2	55 ± 5
$PEtPh_2$	0.63	111 ± 1	50 ± 4
PMe_2Ph	0.55	108 ± 2	38 ± 5
PEt_3	0.20	113 ± 3	46 ± 9
PCy_3	0.48	113 ± 2	53 ± 6
s-$PhobPC_5$	1.38	109 ± 10	51 ± 34
a_5-$PhobPC_5$	4.71	101 ± 2	35 ± 5
Lim-C_5	1.59	106 ± 3	42 ± 10
Lim-C_{18}	1.66	109 ± 3	52 ± 8
PPh_3 (R = ^{n}Pr)	0.92	115 ± 6	66 ± 17
Lim-C_{18} (R = ^{n}Pr)	1.91	106 ± 4	44 ± 13

[a]R = Me except where stated.

Variable temperature measurements resulted in satisfactory linear Eyring plots, giving the activation parameters in Table 2. Notably, the values of $\Delta H^{\ddagger}$ are significantly larger than those obtained in the hydrogenolysis study (Table 1), and the values of $\Delta S^{\ddagger}$ are positive, consistent with rate-determining CO dissociation. The smallest $\Delta H^{\ddagger}$ is found for $[Co(CO)_3(a_5\text{-}PhobPC_5)(COMe)]$, the most reactive complex, but values of $\Delta H^{\ddagger}$ for all complexes span quite a narrow range (101−113 kJ mol^{-1}). A rate constant (1.3×10^{-4} s^{-1}) calculated at 25 °C for $[Co(CO)_3(PPh_3)(COMe)]$ using the activation parameters is in reasonable agreement with the value (1.11×10^{-4} s^{-1}) previously reported by Wegman.[44]

Kinetic experiments were also carried out using toluene as the solvent, and values of k_{obs} were found to be ∼20% higher than in THF but following the same trend with variation of L. The *n*-butyryl complexes, $[Co(CO)_3(L)(CO^nPr)]$ (L = PPh_3, $LimPC_{18}$), were found to have rates only marginally different from the acetyl analogues.

Discussion of Ligand Effects. As noted earlier, the effect of a coordinated phosphine ligand L on the lability of a CO ligand arises from a combination of electronic and steric properties of L. A convenient measure of the electron donor strength of a phosphine ligand is provided by the C−O stretching vibrational frequencies of a metal carbonyl complex, as exemplified by Tolman's electronic parameter for the $[Ni(CO)_3L]$ system.[46] Values of k_{obs} for the reactions of $[Co(CO)_3(L)(COMe)]$ with Ph_3SnH are plotted against ν(CO) for the reactant complex in Figure 6. For five of the complexes, there is a good linear correlation, denoted by the dashed line, such that weaker donation by the phosphine (i.e., increasing ν(CO)) results in larger k_{obs}, in the order PEt_3 < PMe_2Ph < $PEtPh_2$ < PPh_3 < $P(4\text{-}ClC_6H_4)_3$. The trend within this series can be accounted for by the electronic effect of the phosphine on Co−CO backbonding.

The k_{obs} values for the other complexes in Figure 6 are higher than would be expected if only electronic effects were in operation. These data points all belong to relatively bulky phosphines, indicating that steric congestion can also play a significant role in promoting CO dissociation. The most obvious outlier point is for L = a_5-$PhobPC_5$, which also gave the fastest rate in the hydrogenolysis reactions. It is again notable that the promotional effect of the a_5-$PhobPC_5$ isomer on CO dissociation is substantially higher than for the *s*-$PhobPC_5$ ligand. The slightly weaker donor strength of the a_5 isomer may contribute to this difference, but steric effects are likely dominant.

dx.doi.org/10.1021/cs300589n | ACS Catal. 2012, 2, 2512−2523

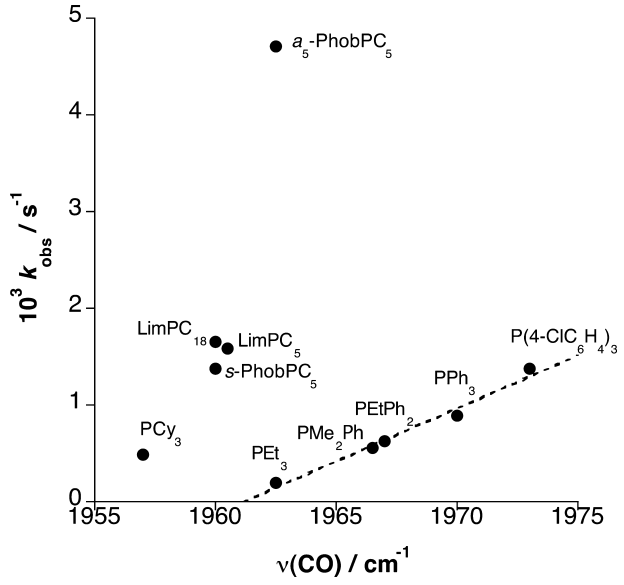

Figure 6. Plot of k_{obs} values for reactions of $[Co(CO)_3(L)(COMe)]$ with Ph_3SnH (74 mM, THF, 40 °C) versus ν(CO) of the reactant complex (average of the two components of the split E mode). The dashed line represents the best linear fit to the data points for L = PEt_3, PMe_2Ph, $PEtPh_2$, PPh_3, and $P(4\text{-}ClC_6H_4)_3$.

The most widely used measure of ligand steric bulk is Tolman's cone angle.[46] A previous study determined the cone angle for both *s*-PhobPR and a_5-PhobPR ligands on the basis of the X-ray crystal structures of the corresponding phosphine selenides and found them to be very similar for the two isomeric forms (in the range 165−175°).[10] Although the cone angle is an intuitively straightforward measure of ligand steric bulk, it is perhaps most appropriate for simple PR_3 ligands rather than those with bicyclic structures, such as PhobPR and LimPR. An alternative is the He_8_steric parameter introduced recently by Fey et al.[47] This is determined by computation of the interaction energy between the ligand and a ring of eight He atoms held in fixed positions on a circle of radius 2.5 Å with its centroid 2.28 Å from the phosphorus atom. Reported values of the He_8_steric parameter (in kcal mol^{-1}) for *s*-PhobPME and a_5-PhobPME are 4.8 and 3.7 respectively, indicating that the a_5 isomer is more sterically demanding.[11] This supports the notion that greater steric congestion contributes to the high reactivity of $[Co(CO)_3(a_5\text{-}PhobPC_5)(COMe)]$. Steric effects have been noted for other reactions of metal complexes involving CO dissociation, such as CO substitution in $[Ni(CO)_3L]$,[48] *cis*-$[Mn(CO)_4LBr]$,[49] $[Ru(CO)_3L(SiCl_3)_2]$,[50] and $[Ru(CO)_4L]$ [51] and decarbonylation of $[Mo(CO)_2(L)(COMe)(\eta^5\text{-}C_5H_5)]$.[52]

X-ray Structures of $[Co(CO)_3L]_2$ (L = s-PhobPC$_5$ and a_5-PhobPC$_5$). Crystallographic studies of a number of cobalt dimers, $[Co(CO)_3(L)]_2$, have been reported previously, including several examples for L = *s*-PhobPR (R = Et, $^nC_5H_{11}$, Cy, $C_3H_6NMe_2$) in a study by Bungu and Otto.[12] During the course of the present work, a new structure was obtained for $[Co(CO)_3(s\text{-}PhobPC_5)]_2$ as well as for the isomeric $[Co(CO)_3(a_5\text{-}PhobPC_5)]_2$ (illustrated in Figures 7 and 8 respectively). The two structures for the *s*-$PhobPC_5$ complex closely resemble each other, apart from some disorder in the positions of C_3−C_5 of one of the pentyl chains in the previously published case.

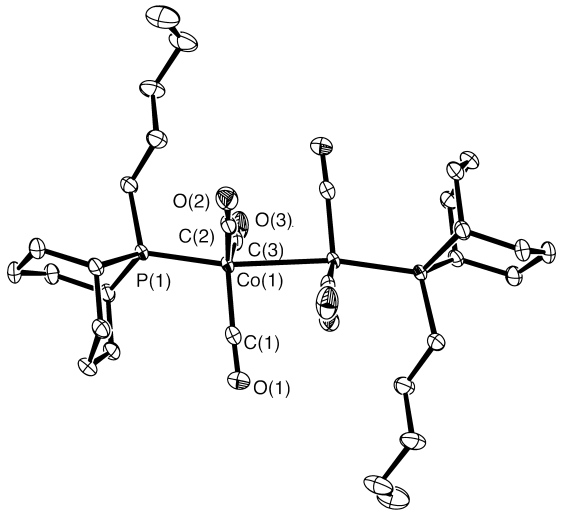

Figure 7. ORTEP diagram showing the molecular structures of $[Co(CO)_3(s\text{-}PhobPC_5)]_2$. Thermal ellipsoids are shown at the 50% probability level, and hydrogen atoms are omitted. Selected bond distances (Å): Co1−C1, 1.793(3); Co1−C2, 1.783(4); Co1−C3, 1.772(4); Co1−Co1′, 2.6712(8); Co1−P1, 2.22012(8). Selected bond angles (°): P1−Co1−Co1′, 168.75(3); P1−Co1−C1, 103.46(10); P1−Co1−C2, 91.10(10); P1−Co1−C3, 88.91(10); C1−Co1−C2, 114.74(15); C2−Co1−C3, 125.66(16); C3−Co1−C1, 118.00(17).

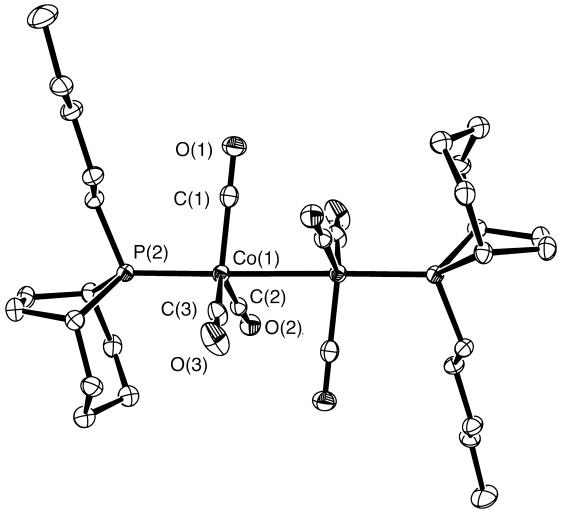

Figure 8. ORTEP diagram showing the molecular structure of $[Co(CO)_3(a_5\text{-}PhobPC_5)]_2$. Thermal ellipsoids are shown at the 50% probability level, and hydrogen atoms are omitted. Selected bond distances (Å): Co1−C1, 1.7899(19); Co1−C2, 1.7868(19); Co1−C3, 1.7858(19); Co1−Co1′, 2.6862(5); Co1−P2, 2.2173(5). Selected bond angles (°): P2−Co1−Co1′, 179.16(2); P2−Co1−C1, 95.56(6); P2−Co1−C2, 98.29(6); P2−Co1−C3, 93.34(6); C1−Co1−C2, 116.50(8); C2−Co1−C3, 123.75(9); C3−Co1−C1, 116.78(8).

In both structures, each cobalt center adopts approximately trigonal bipyramidal geometry with the phosphine coordinated trans to the Co−Co bond and the three CO ligands in equatorial positions; hence, the coordination environment can be regarded as a useful model for the acyl species $[Co(CO)_3(L)(COR)]$. It is instructive to inspect the structures for any distortions that might arise from steric strain. For $[Co(CO)_3(s\text{-}PhobPC_5)]_2$, the P−Co−Co angle (∼169°) deviates significantly from linearity, and one of the P−Co−CO angles is ∼103.5°, with an average of 94.5°. For

dx.doi.org/10.1021/cs300589n | ACS Catal. 2012, 2, 2512−2523

$[Co(CO)_3(a_5\text{-PhobPC}_5)]_2$, the P−Co−Co angle is almost linear (179°), and the largest P−Co−CO angle is 98.3°. However, it is notable in this structure that all three P−Co−CO angles are significantly greater than 90°, with an average of 95.7°.[53] Inspection of space-filling models indicates that for the $[Co(CO)_3(s\text{-PhobPC}_5)]_2$ structure, the single large P−Co−CO angle results from relatively close contact between a CO ligand and two hydrogens from one of the 6-membered rings of the phobane ligand, as illustrated in Chart 2a. In the $[Co(CO)_3(a_5\text{-PhobPC}_5)]_2$ structure, the 7-membered ring of the phobane ligand directs three hydrogens toward a pair of CO ligands, pushing them out of the equatorial plane (Chart 2b). Although it is difficult to draw strong conclusions from subtle differences in geometrical parameters, these apparent distortions are consistent with the suggestion that steric effects of these ligands could cause enhanced CO lability. A particular feature of the PhobPR and LimPR ligands (compared with PCy_3, for example) is the absence of 3-fold symmetry about the M−C axis. This will create regions of greater steric congestion, as depicted in Chart 2 for the phobanes, and has been noted to result in restricted rotation of the phosphine ligands in a ruthenium complex, $[Ru(=CHPh)Cl_2(s\text{-PhobPCy})_2]$.[54]

Chart 2. Schematic Showing Steric Congestion between CO Ligands and Phobane Ligands in $[Co(CO)_3(L)]_2$ Complexes (a) L = *s*-PhobPR and (b) L = a_5-PhobPR

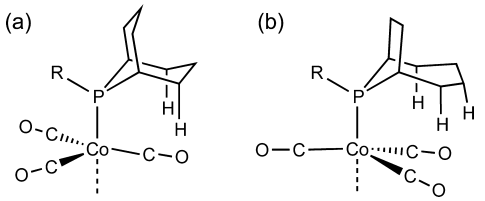

Computational Results. Calculations using density functional theory (DFT) were also used to explore the ligand effects observed in this investigation. Geometry optimizations were performed for selected acetyl complexes, $[Co(CO)_3(L)(COMe)]$, and the dicarbonyl species resulting from CO loss. The coordinatively unsaturated product can adopt either an η^2-acyl or a β-agostic C−H−Co structure (Chart 3) to stabilize the vacant site, as found for $[Co(CO)_3(COR)]$ in theoretical studies of the unmodified system.[37−39,55] The coordinates and energies for optimized structures are given in the Supporting Information. In all cases, the η^2-acyl isomer of $[Co(CO)_2(L)(COMe)]$ is calculated to be lower in energy by ∼10−20 kJ mol^{-1} relative to the β-agostic complex. This concurs with evidence from flash photolysis experiments that supports the η^2-acyl structure for $[Co(CO)_2(L)(COMe)]$.[43]

Chart 3. Alternative Structures of CO Dissociation Product, $[Co(CO)_2(L)(COMe)]$

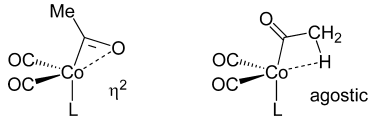

Calculated energies of CO dissociation for a range of $[Co(CO)_3(L)(COMe)]$ complexes are given in Table 3. It is notable that the highest ΔH and ΔG values are for the complex with L = PMe_3 and that CO dissociation becomes more favorable on progression to less basic phosphines by sequential replacement of methyls by phenyl groups. This trend continues on introduction of *para*-chloro or -fluoro substituents. Steric effects are clearly apparent, with much lower ΔH and ΔG values for complexes of bulky ligands such as P(*o*-tolyl)$_3$ and P^{t}Bu$_3$ (not studied experimentally) and to a lesser extent for PCy_3. Most interesting in relation to the experimental data is the difference in calculated CO dissociation energies for the *s*-PhobPME and a_5-PhobPME complexes (with methyl replacing pentyl in the computational model). CO dissociation from the a_5-PhobPME complex is calculated to be ∼10 kJ mol^{-1} more favorable than from the *s*-PhobPME analogue, which is in line with the experimental observations. The two LimPME stereoisomers are marginally different, but neither is predicted to facilitate CO loss as much as the *s*- and a_5-phobane isomers. Out of curiosity, calculations were also performed on the a_7-PhobPME system (not studied experimentally), and it was found to have a higher CO dissociation energy than either the *s*- or a_5 isomers. This is in accord with previous studies that suggest the a_7 species is the strongest donor and least sterically hindered of the three phobane isomers.[11] These DFT results provide additional support for the experimental evidence that phosphine ligands tune the reactivity of $[Co(CO)_3(L)(COMe)]$ toward hydrogenolysis and related reactions by influencing the labillity of a CO ligand via electronic and steric effects.

Table 3. DFT Calculated Energies (B3LYP, SDD) for CO dissociation from $[Co(CO)_3(L)(COMe)]$ To Give η^2-Acetyl or Agostic Isomer of $[Co(CO)_2(L)(COMe)]$

	η^2-acetyl product		agostic product	
L	ΔH /kJ mol^{-1}	ΔG /kJ mol^{-1}	ΔH /kJ mol^{-1}	ΔG /kJ mol^{-1}
PMe_3	109.0	61.2	123.4	79.1
PMe_2Ph	107.0	59.9	122.1	78.2
$PMePh_2$	104.5	56.0	121.4	75.0
PPh_3	102.7	56.6	114.4	71.5
$P(4\text{-}ClC_6H_4)_3$	100.1	52.6	114.2	70.3
$P(4\text{-}FC_6H_4)_3$	99.3	52.9	114.3	70.9
P(*o*-tol)$_3$	86.8	36.0	104.4	56.2
P^{t}Bu$_3$	76.4	25.2	99.4	52.0
PCy_3	94.9	46.7	112.9	67.7
s-PhobPME	95.6	46.1	115.0	69.2
a_5-PhobPME	85.3	36.7	106.3	58.7
a_7-PhobPME	102.4	52.5	120.0	73.4
LimPME[a]	97.2, 97.3	50.7, 50.8	115.9, 116.0	70.7, 71.0

[a]Two values are for LimPME ligand with 4-*R* and 4-*S* stereochemistry respectively.

CONCLUSIONS

The results presented in this paper illustrate the application of in situ IR spectroscopy to obtain kinetic data for an important step in phosphine-modified cobalt hydroformylation catalysis at moderate temperature and pressure. The rate of hydrogenolysis of cobalt acyls is shown to depend markedly on the stereoelectronic properties of the coordinated phosphine ligand. The data are consistent with the established CO-loss mechanism for this reaction step, as further supported by ^{13}CO isotopic exchange experiments and model reactions using Ph_3SnH. For phosphines of relatively low steric bulk, the rate of CO loss from $[Co(CO)_3(L)(COR)]$ is largely governed by electronic properties of the phosphine L; hence, more strongly donating phosphines inhibit CO dissociation by enhancing

dx.doi.org/10.1021/cs300589n | ACS Catal. 2012, 2, 2512−2523

Co−CO backbonding. However, higher reactivity can be induced for strong donor ligands by introduction of greater steric bulk or rigidity. For example, in PCy_3 and bicyclic phobane or limonene-derived phosphines, the loss of a CO ligand appears to be facilitated by relief of steric congestion. The most notable example of this effect is for the a_5-PhobPC_5 ligand, which confers significantly higher reactivity than the *s*-PhobPC_5 isomer. The experimental observations are also supported by DFT calculations on the thermodynamics of CO loss from $[Co(CO)_3(L)(COMe)]$.

It is not straightforward to link the results of this study directly to the observed effects of phosphine ligands in catalytic hydroformylation. Whereas hydrogenolysis of $[Co(CO)_4(COR)]$ has been proposed as the rate-limiting step for the unmodified cobalt catalyst, in phosphine-modified systems, the dissociative substitution of CO by alkene in $[Co(CO)_3(L)H]$ is thought to become rate-limiting. However, recent studies have suggested this is an oversimplification and that for certain large symmetrical ligands (e.g., PCy_3), the carbonylation step may contribute.[13] Hence, the overall catalytic rate will depend on a number of rate/equilibrium constants, and each of these will vary with the properties of the phosphine ligand L. Despite the complexity, it is to be expected that overall catalytic activity will be related to the lability of the metal complexes involved. Dissociation of CO from the hydride $[Co(CO)_3(L)H]$ at the start of the cycle is likely to show a dependence on the properties of L similar to that found in this study for CO loss from $[Co(CO)_3(L)(COR)]$. Alkane formation via hydrogenolysis of $[Co(CO)_3(L)R]$ would also be expected to show a trend similar to that for hydrogenolysis of cobalt acyls. However, the alkane forming side reaction is competitive with the carbonylation of $[Co(CO)_3(L)R]$, which will also be affected by L. Although the catalytic behavior cannot be inferred directly from the results of this study, it is notable that the most reactive cobalt acyl complexes are those that contain phosphine ligands (e.g., PhobPR and LimPR) that impart high catalytic rates. The unsymmetrical nature of these ligands, with specific regions of steric congestion, may be important for this behavior.

EXPERIMENTAL SECTION

Materials. The solvents toluene, diethyl ether, petroleum ether, dichloromethane, 1,2-dichloroethane, hexane, and tetrahydrofuran were supplied from a Grubbs solvent purification system and stored under N_2.[56] The PhobPC_5 and Lim$PC_{5/18}$ ligands were synthesized using literature methods,[10,16] and samples were purified from oxidation products when necessary by passing a solution in toluene through a short silica column. The Lim$PC_{5/18}$ ligands were used as a mixture of diastereoisomers. Other phosphine ligands and triphenyltinhydride were supplied by Sigma-Aldrich and were used without further purification. $[Co_2(CO)_8]$ was supplied by Strem Chemicals and stabilized with 1−5% hexane. Hydrogen (99.9995% HP grade) and carbon monoxide (99.9% CP grade) were supplied by BOC. ^{13}C-enriched carbon monoxide (99% ^{13}C) was supplied by Euriso-Top. Methyl iodide (Sigma-Aldrich) was distilled over calcium hydride and stored at 5 °C in a foil-wrapped Schlenk tube under nitrogen and over mercury.

Instrumentation. FT-IR spectra were recorded using a Perkin-Elmer Spectrum GX spectrometer controlled by Spectrum and Timebase software or a Mattson Genesis Series spectrometer controlled by WinFirst software. Routine solution spectra were recorded using a 0.5 mm path length liquid cell with CaF_2 windows. High-pressure/high-temperature IR spectra were recorded using a SpectraTech Cylindrical Internal Reflectance (CIR) cell (vide infra). For these experiments, a liquid-nitrogen-cooled MCT detector was used on the Perkin-Elmer Spectrum GX spectrometer to afford high sensitivity. NMR spectra were recorded on either a Bruker AC250 or AC400 spectrometer fitted with an automatic sample changer and operating in pulse Fourier transform mode using the solvent as reference. Spectra were analyzed using Bruker 1D WINNMR software. Negative ion electrospray mass spectrometry was performed using a Waters LCT time-of-flight instrument. GC/MS measurements were made using a Perkin-Elmer AutoSystem GC instrument connected to a TurboMass mass spectrometer. Elemental analyses were performed using a Perkin-Elmer 2400 Elemental Analyzer.

Synthetic Methods. Cobalt acetyl complexes $[Co(CO)_3(L)(COMe)]$ were synthesized using established literature methods.[57−59] A generic example for L = PPh_3 is described as follows. $[Co_2(CO)_8]$ (2.61 g, 7.63 mmol) and powdered NaOH (9.92 g, 0.248 mol) were placed in an N_2-filled flask to which THF (100 cm^3) was added. The reaction mixture was stirred vigorously for 1 h, and the resulting pale yellow solution was filtered through Celite via cannula. After cooling the solution containing $Na[Co(CO)_4]$ to −78 °C, methyl iodide (10 cm^3, 0.16 mol) was added by syringe. After stirring for 1 h, the methyl iodide was removed under vacuum, and PPh_3 (3.84 g, 14.65 mmol) dissolved in THF (10 cm^3) was added via syringe. The solution was allowed to stir for 30 min before introduction of an atmosphere of carbon monoxide and stirring for a further 12 h. The solvent was removed, and the solid residue was extracted into diethyl ether. Flash filtration through an alumina column topped with Celite gave a deep yellow/orange solution. The product was isolated as yellow crystals by layering hexane onto the diethyl ether solution and cooling to −4 °C for 6 days (yield 4.345 g, 63%). Alternatively, a method similar to that described by Tso and Cutler[59] was used, whereby the dimer $[Co(CO)_3(PPh_3)]_2$ was reduced to $Na[Co(CO)_3(PPh_3)]$ using sodium amalgam, followed by sequential reaction with methyl iodide and carbon monoxide. For *n*-butyryl complexes, $[Co(CO)_3(L)(CO^nPr)]$, the procedure described above was adapted by adding butyryl chloride to the THF solution of $Na[Co(CO)_4]$ at 0 °C, then allowing this to warm to room temperature, followed by addition of PPh_3 dissolved in THF. Dimers of the type $[Co(CO)_3L]_2$ were prepared using the method of Tso and Cutler.[59] Spectroscopic data for cobalt complexes are given in Table 4.

Kinetics of Hydrogenolysis Reactions. Reactions of $[Co(CO)_3(L)(COR)]$ with hydrogen were monitored in situ by high-pressure IR spectroscopy using a cylindrical internal reflectance (CIR) cell comprising an autoclave (Parr) modified (by SpectraTech) to accommodate a crystalline silicon CIR rod, as described by Moser.[32−36] Spectra were recorded using a Perkin-Elmer Spectrum GX FTIR spectrometer fitted with an MCT detector. The cell was placed directly in the spectrometer sample compartment and aligned to maximize IR energy throughput using a tilt table. A background spectrum for each experiment was recorded using the appropriate solvent and temperature. The reaction solution was prepared by dissolving the cobalt compound $[Co(COR)(CO)_3(L)]$ (~0.14 g, 0.35 mmol) in 8 cm^3 of toluene and then added to the cell, to which the head was then fitted securely and the stirrer activated (285 rpm). The cell was flushed at least four times with H_2 before

dx.doi.org/10.1021/cs300589n | ACS Catal. 2012, 2, 2512−2523

Table 4. IR and ^{31}P NMR Spectroscopic Data for Cobalt Acyl Complexes $[Co(CO)_3(L)(COR)]$

L	R	ν(CO)/cm^{-1}	δ ^{31}P
PPh_3	Me	2048, 1979, 1961, 1669	49.3
$P(4\text{-}ClC_6H_4)_3$	Me	2051, 1982, 1964, 1675	48.8
$PMePh_2$	Me	2047, 1976, 1959, 1668	33.4
$PEtPh_2$	Me	2046, 1976, 1958, 1667	46.1
PMe_2Ph	Me	2046, 1975, 1958, 1665	18.8
PEt_3	Me	2043, 1971, 1954, 1662	42.2
P^nBu_3	Me	2042, 1971, 1953, 1660	34.6
PCy_3	Me	2038, 1966, 1948, 1659	61.5
s-PhobPC$_5$	Me	2041, 1970, 1950, 1664	27.4
a_5-PhobPC$_5$	Me	2043, 1973, 1952, 1668	54.0
LimPC$_5$	Me	2041, 1970, 1951, 1662	21.0, 18.8[a]
LimPC$_{18}$	Me	2042, 1970, 1950, 1662	20.9, 18.8[a]
s-PhobPC$_5$	^{n}Pr	2038, 1968, 1946, 1666	27.4
PPh_3	^{n}Pr	2046, 1977, 1958, 1671	49.2
$PMePh_2$	^{n}Pr	2045, 1974, 1956, 1669	33.2
LimPC$_{18}$	^{n}Pr	2039, 1968, 1948, 1665	20.6, 18.5[a]

[a]Two signals arise from the presence of two diastereoisomers of the LimPC$_{5/18}$ ligands

filling to the desired H_2 pressure and heating to the reaction temperature. Spectra recorded over the range 2200−1600 cm^{-1} at regular intervals under computer control and absorbance vs time data for the appropriate ν(CO) bands were extracted and analyzed off-line using Kaleidagraph curve-fitting software. Exponential fits to the decay traces gave pseudo-first-order rate constants (listed in the Supporting Information) that were reproducible within ±10%.

Kinetics for Ph_3SnH Reactions. Samples for kinetic analysis of the reactions of $[Co(CO)_3(L)(COR)]$ with triphenyltin hydride were prepared by placing the required amount of Ph_3SnH in a 2 cm^3 graduated flask, which was then filled up to the mark with THF or toluene. A portion of this solution was used to record a background spectrum. Another portion (typically 500 μL) was added to the solid metal complex (typically ∼2 mg) in a sample vial to give a reaction solution with a complex concentration of ∼10 mM. A portion of the reaction solution was quickly transferred to the IR cell (0.5 mm path length, CaF_2 windows), which was maintained at constant temperature throughout the kinetic run by a thermostatted jacket. Spectra were scanned in the ν(CO) region (2200−1600 cm^{-1}) and saved at regular time intervals under computer control. After the kinetic run, absorbance vs time data for the appropriate ν(CO) frequencies were extracted and analyzed off-line using Kaleidagraph curve-fitting software. Exponential fits to the decay traces had correlation coefficients of ≥0.999, giving pseudo-first -order rate constants (listed in the Supporting Information) that were reproducible within ±5%.

^{13}CO Isotopic Exchange Experiments. $[Co(COMe)(CO)_3(PPh_3)]$ (30 mg, 66.5 μmol) was dissolved in 1,2-dichloroethane (10 cm^3) and added to a flask filled with ^{13}CO. The solution was stirred vigorously and maintained at 50 °C using a temperature-controlled water bath. During the course of the reaction, samples were taken at known time periods and analyzed immediately by IR. An analogous procedure was employed for $[Co(COMe)(CO)_3(s\text{-}PhobPC_5)]$.

X-ray Crystallography. Data were collected on a Bruker Smart Apex II CCD area detector with a Oxford Cryostream 600 low temperature system (150 K) using Mo K_α radiation (λ = 0.71073 Å). The structures were solved by direct methods and refined by full matrix least-squares methods on F^2. Hydrogen atoms were placed geometrically and refined using a riding model (including torsional freedom for methyl groups). Complex scattering factors were taken from the SHELXTL program package.[85] Crystallographic data are summarized in Table 5, and cif files are provided in the Supporting Information.

Computational Details. Density functional theory (DFT) calculations were performed using the Gaussian 09 program packages,[60] compiled using the Portland compiler (version 8.0-2) on an EMT64 architecture using Gaussian-supplied versions of BLAS and ATLAS. All calculations were in vacuo and employed the B3LYP functional[61] with Stuttgart/Dresden pseudopotentials[62,63] on cobalt and the D95 V basis set[64] on all other atoms, supplemented by extra *d* functions on phosphorus (exponent 0.60) and chlorine (exponent 0.75).

Table 5. Summary of Crystallographic Data

	$[Co(CO)_3(PEtPh_2)(COMe)]$	$[Co(CO)_3(s\text{-}PhobPC_5)]_2$	$[Co(CO)_3(a_5\text{-}PhobPC_5)]_2$
empirical formula	$C_{19}H_{18}CoO_4P$	$C_{16}H_{25}CoO_3P$	$C_{32}H_{50}Co_2O_6P_2$
formula weight	400.23	355.26	710.52
T/K	150(2)	150(2)	150(2)
crystal system	orthorhombic	triclinic	monoclinic
space group	*Pna*2$_1$	*P*-1	*P*2$_1$/*n*
a/Å	14.5719(15)	9.0646(8)	12.6461(5)
b/Å	17.2445(18)	9.2649(8)	9.7325(4)
c/Å	7.3877(8)	11.4599(10)	14.7834(5)
α/deg	90	94.012(6)	90
β/deg	90	108.645(5)	110.949(2)
γ/deg	90	109.326(5)	90
V/Å^3	1856.4(3)	843.74(13)	1699.24(11)
Z	4	2	2
μ/mm^{-1}	1.030	1.118	1.110
crystal size/mm	0.43 × 0.23 × 0.23	0.20 × 0.12 × 0.10	0.23 × 0.21 × 0.10
no. of rflxns: total/indep (R_{int})	15355/4136 (0.0289)	16698/4758 (0.0391)	28790/3903 (0.0339)
final *R*1	0.0279	0.0592	0.0295
largest peak, hole/e Å^{-3}	0.374, −0.227	2.800, −0.632	0.617, −0.286

dx.doi.org/10.1021/cs300589n | ACS Catal. 2012, 2, 2512−2523

Geometry optimizations were performed using the default settings. No correction was made for basis set superposition error as the two outcomes of CO dissociation result in fragments that are isomeric. For complexes where more than one local minimum structure was located, the data reported are for the structure of lowest energy.

■ ASSOCIATED CONTENT

Supporting Information

Kinetic data, Eyring plots, coordinates, and energies for DFT optimized structures (pdf), and crystallographic data (cif). This information is available free of charge via the Internet at http://pubs.acs.org/.

■ AUTHOR INFORMATION

Corresponding Author

*E-mail: a.haynes@sheffield.ac.uk.

Notes

The authors declare no competing financial interest.

■ ACKNOWLEDGMENTS

Financial support from Sasol Technology Research & Development (studentship to J.M.B.) is gratefully acknowledged. Dr Anthony Meijer is thanked for advice on the DFT calculations.

■ REFERENCES

(1) Beller, M.; Cornils, B.; Frohning, C. D.; Kohlpaintner, C. W. *J. Mol. Catal.* **1995**, *104*, 17.
(2) Bohnen, H.-W.; Cornils, B. *Adv. Catal.* **2002**, *47*, 1.
(3) Van Leeuwen, P. W. N. M. In *Homogeneous Catalysis: Understanding the Art*; 1st ed.; Springer: Dordrecht, 2005.
(4) Wiese, K.-D.; Obst, D. *Top. Organomet. Chem.* **2006**, *18*, 1.
(5) Hebrard, F.; Kalck, P. *Chem. Rev.* **2009**, *109*, 4272.
(6) Heck, R. F.; Breslow, D. S. *J. Am. Chem. Soc.* **1961**, *83*, 4023.
(7) Van Winkle, J. L.; Lorenzo, S.; Morris, R. C.; Mason, R. F. U.S. Patent 3420898, 1969.
(8) Eberhard, M. R.; Carrington-Smith, E.; Drent, E. E.; Marsh, P. S.; Orpen, A. G.; Phetmung, H.; Pringle, P. G. *Adv. Synth. Catal.* **2005**, *347*, 1345.
(9) Lewis, J. C.; Wu, J. Y.; Bergman, R. G.; Ellman, J. A. *Angew. Chem., Int. Ed.* **2006**, *45*, 1589.
(10) Bungu, P. N.; Otto, S. *J. Organomet. Chem.* **2007**, *692*, 3370.
(11) Carreira, M.; Charernsuk, M.; Eberhard, M.; Fey, N.; Van Ginkel, R.; Hamilton, A.; Mul, W. P.; Orpen, A. G.; Phetmung, H.; Pringle, P. G. *J. Am. Chem. Soc.* **2009**, *131*, 3078.
(12) Bungu, P. N.; Otto, S. *Dalton Trans.* **2007**, 2876.
(13) Bungu, P. N.; Otto, S. *Dalton Trans.* **2011**, *40*, 9238.
(14) Robertson, A.; Bradaric, C.; Frampton, C. S.; McNulty, J.; Capretta, A. *Tetrahedron Lett.* **2001**, *42*, 2609.
(15) Steynberg, J. P.; Govender, K.; Steynberg, P. J. World Patent WO0214248, 2002.
(16) Crause, C.; Bennie, L.; Damoense, L.; Dwyer, C. L.; Grove, C.; Grimmer, N.; Janse van Rensburg, W.; Kirk, M. M.; Mokheseng, K. M.; Otto, S.; Steynberg, P. J. *Dalton Trans.* **2003**, 2036.
(17) Polas, A.; Wilton-Ely, J. D. E. T.; Slawin, A. M. Z.; Foster, D. F.; Steynberg, P. J.; Green, M. J.; Cole-Hamilton, D. J. *Dalton Trans.* **2003**, 4669.
(18) Damoense, L.; Datt, M.; Green, M.; Steenkamp, C. *Coord. Chem. Rev.* **2004**, *248*, 2393.
(19) Dwyer, C.; Assumption, H.; Coetzee, J.; Crause, C.; Damoense, L.; Kirk, M. *Coord. Chem. Rev.* **2004**, *248*, 653.
(20) Whyman, R. *J. Organomet. Chem.* **1974**, *66*, C23.
(21) Whyman, R. *J. Organomet. Chem.* **1974**, *81*, 97.
(22) Whyman, R. *J. Organomet. Chem.* **1975**, *94*, 303.
(23) Van Boven, M.; Alemdaroglu, N.; Penninger, J. M. L. *J. Organomet. Chem.* **1975**, *84*, 65.
(24) Kramarz, K. W.; Klingler, R. J.; Fremgen, D. E.; Rathke, J. W. *Catal. Today* **1999**, *49*, 339.
(25) Klingler, R. J.; Chen, M. J.; Rathke, J. W.; Kramarz, K. W. *Organometallics* **2007**, *26*, 352.
(26) Darensbourg, D. J.; Phelps, A. L.; Le Gall, N.; Jia, L. *J. Am. Chem. Soc.* **2004**, *126*, 13808.
(27) Xu, H.; Legall, N.; Jia, L.; Brennessel, W. W.; Kucera, B. E. *J. Organomet. Chem.* **2005**, *690*, 5150.
(28) Llewellyn, S. A.; Green, M. L. H.; Cowley, A. R. *J. Organomet. Chem.* **2005**, *690*, 2358.
(29) Piacenti, F.; Bianchi, M.; Benedetti, E. *Chim. Ind.* **1967**, *49*, 245.
(30) Martin, J. T.; Baird, M. C. *Organometallics* **1983**, *2*, 1073.
(31) Kovács, I.; Ungváry, F.; Markó, L. *Organometallics* **1986**, *5*, 209.
(32) Moser, W. R.; Cnossen, J. E.; Wang, A. W.; Krouse, S. A. *J. Catal.* **1985**, *95*, 21.
(33) Moser, W. R.; Papile, C. J.; Brannon, D. A.; Duwell, R. A.; Weininger, S. J. *J. Mol. Catal.* **1987**, *41*, 271.
(34) Moser, W. R.; Papile, C. J.; Weininger, S. J. *J. Mol. Catal.* **1987**, *41*, 293.
(35) Moser, W. R.; Marshik-Guerts, B. J.; Okrasinski, S. J. *J. Mol. Catal. A: Chem.* **1999**, *143*, 57.
(36) Moser, W. R.; Marshik-Guerts, B. J.; Okrasinski, S. J. *J. Mol. Catal. A: Chem.* **1999**, *143*, 71.
(37) Solà, M.; Ziegler, T. *Organometallics* **1996**, *15*, 2611.
(38) Huo, C. F.; Li, Y. W.; Beller, M.; Jiao, H. *Organometallics* **2003**, *22*, 4665.
(39) Maeda, S.; Morokuma, K. *J. Chem. Theory Comput.* **2012**, *8*, 380.
(40) Brunner, E. *J. Chem. Eng. Data* **1985**, *30*, 269.
(41) A $^{13}C\{^{1}H\}$ NMR spectrum recorded after the ^{13}CO exchange experiment showed the expected resonances for the fully labelled product, $[Co(^{13}CO)_3(s\text{-}PhobPC_5)(^{13}COMe)]$: δ 184.2 (Co−**C**O); 200.4 (Co−**C**OMe).
(42) Hoff, C. D.; Ungváry, F.; King, R. B.; Markó, L. *J. Am. Chem. Soc.* **1985**, *107*, 666.
(43) Massick, S. M.; Buttner, T.; Ford, P. C. *Inorg. Chem.* **2003**, *42*, 575.
(44) Wegman, R. W. *Organometallics* **1986**, *5*, 707.
(45) Gregg, B. T.; Cutler, A. R. *Organometallics* **1992**, *11*, 4276.
(46) Tolman, C. A. *Chem. Rev.* **1977**, *77*, 313.
(47) Fey, N.; Tsipis, A. C.; Harris, S. E.; Harvey, J. N.; Orpen, A. G.; Mansson, R. A. *Chem.—Eur. J.* **2006**, *12*, 291.
(48) Meriwether, L. S.; Fiene, M. L. *J. Am. Chem. Soc.* **1959**, *81*, 4200.
(49) Angelici, R. J.; Basolo, F. *Inorg. Chem.* **1963**, *2*, 728.
(50) Chalk, K. L.; Pomeroy, R. K. *Inorg. Chem.* **1984**, *23*, 444.
(51) Chen, L.; Poe, A. J. *Inorg. Chem.* **1989**, *28*, 3641.
(52) Barnett, K. W.; Pollmann, T. G. *J. Organomet. Chem.* **1974**, *69*, 413.
(53) For the corresponding dimer with L = PCy_3, P−Co−Co = 175.855(13)° and P−Co−CO (avg) = 95.14(4)° (range 92.29(4)−96.79(4)°). For L = $LimPC_{18}$, P−Co−Co = 177.87(7)° and 170.23(8)° and P−Co−CO (avg) = 94.6(3)° (range 88.6(3)−96.9(3)°).
(54) Dwyer, C. L.; Kirk, M. M.; Meyer, W. H.; Janse van Rensburg, W.; Forman, G. S. *Organometallics* **2006**, *25*, 3806.
(55) Goh, S. K.; Marynick, D. S. *Organometallics* **2002**, *21*, 2262.
(56) Pangborn, A. B.; Giardello, M. A.; Grubbs, R. H.; Rosen, R. K.; Timmers, F. J. *Organometallics* **1996**, *15*, 1518.
(57) Kovács, I.; Ungváry, F. *Coord. Chem. Rev.* **1997**, *161*, 1.
(58) Edgell, W. F.; Lyford, J. *Inorg. Chem.* **1970**, *9*, 1932.
(59) Tso, C. C.; Cutler, A. R. *Polyhedron* **1993**, *12*, 149.
(60) Frisch, M. J.; Trucks, G. W.; Schlegel, H. B.; Scuseria, G. E.; Robb, M. A.; Cheeseman, J. R.; Scalmani, G.; Barone, V.; Mennucci, B.; Petersson, G. A.; Nakatsuji, H.; Caricato, M.; Li, X.; Hratchian, H. P.; Izmaylov, A. F.; Bloino, J.; Zheng, G.; Sonnenberg, J. L.; Hada, M.; Ehara, M.; Toyota, K.; Fukuda, R.; Hasegawa, J.; Ishida, M.; Nakajima, T.; Honda, Y.; Kitao, O.; Nakai, H.; Vreven, T.; Montgomery, J. A., Jr.; Peralta, J. E.; Ogliaro, F.; Bearpark, M.; Heyd, J. J.; Brothers, E.; Kudin, K. N.; Staroverov, V. N.; Kobayashi, R.; Normand, J.; Raghavachari, K.; Rendell, A.; Burant, J. C.; Iyengar, S. S.; Tomasi, J.; Cossi, M.; Rega,

N.; Millam, N. J.; Klene, M.; Knox, J. E.; Cross, J. B.; Bakken, V.; Adamo, C.; Jaramillo, J.; Gomperts, R.; Stratmann, R. E.; Yazyev, O.; Austin, A. J.; Cammi, R.; Pomelli, C.; Ochterski, J. W.; Martin, R. L.; Morokuma, K.; Zakrzewski, V. G.; Voth, G. A.; Salvador, P.; Dannenberg, J. J.; Dapprich, S.; Daniels, A. D.; Farkas, Ö.; Foresman, J. B.; Ortiz, J. V.; Cioslowski, J.; Fox, D. J. *Gaussian*, rev. A.02 ed.; Gaussian, Inc.: Wallingford, CT, 2009.

(61) Becke, A. D. *J. Chem. Phys.* **1993**, *98*, 5648.

(62) Nicklass, A.; Dolg, M.; Stoll, H.; Preuss, H. *J. Chem. Phys.* **1995**, *115*, 7348 and references therein.

(63) Cao, X.; Dolg, M. *J. Chem. Phys.* **2001**, *115*, 7348.

(64) Dunning, T. H., Jr.; Hay, P. J. In *Modern Theoretical Chemistry*; Schaefer, H. F., III, Ed.; Plenum: New York, 1976, Vol. *3*, p 1.

NOTE ADDED AFTER ASAP PUBLICATION

After this paper was published online October 31, 2012, a correction was made to the last paragraph of the Results and Discussion section, on page 2519. The corrected version was reposted on November 2, 2012.